ELSEVIER

Geoderma 80 (1997) 353–368

GEODERMA

The use of ^{29}Si MAS-NMR and Monte Carlo methods in the study of Al/Si ordering in silicates

Martin T. Dove *

Department of Earth Sciences, University of Cambridge, Downing Street, Cambridge CB2 3EQ, UK

Received 11 October 1996; accepted 6 January 1997

Abstract

The use of ^{29}Si Magic Angle Spinning NMR to provide information about the local structure and order about the SiO_4 tetrahedra in framework silicates is reviewed. A number of problems, including difficulties of peak assignment and the necessity to measure accurate intensities of the weakest peaks in the NMR spectra, are discussed. ^{29}Si MAS-NMR can be used to determine the number of Al–O–Al linkages in the structure, but the sensitivity of the final answer to experimental errors can lead to absurd results. A new method, involving an inverse Monte Carlo algorithm, to analyse ^{29}Si MAS-NMR data for silicates with long-range Al/Si disorder is described, and illustrated with examples of Cs-leucite, analcime, and annealing measurements for cordierite. © 1997 Elsevier Science B.V.

Keywords: ^{29}Si MAS-NMR; Al/Si order; Monte Carlo; leucite; analcime; cordierite

1. Introduction

^{29}Si Magic Angle Spinning (MAS) NMR is a sensitive probe of the local atomic configuration about the tetrahedral Si sites in aluminosilicate minerals (Kirkpatrick, 1988; Putnis, 1992). An example of the sort of crystal structure we are interested in is shown in Fig. 1: the structure of cordierite, $Mg_2Al_4Si_5O_{18}$, consists of an infinite framework of linked SiO_4 and AlO_4 tetrahedra. There are two important correlations of the MAS-NMR frequency with the local structure, which are shown in Figs. 2 and 3. The first is the correlation with the relative

* Fax: +44 1223-333450; E-mail: martin@minp.esc.cam.ac.uk

PII S0016-7061(97)00060-8

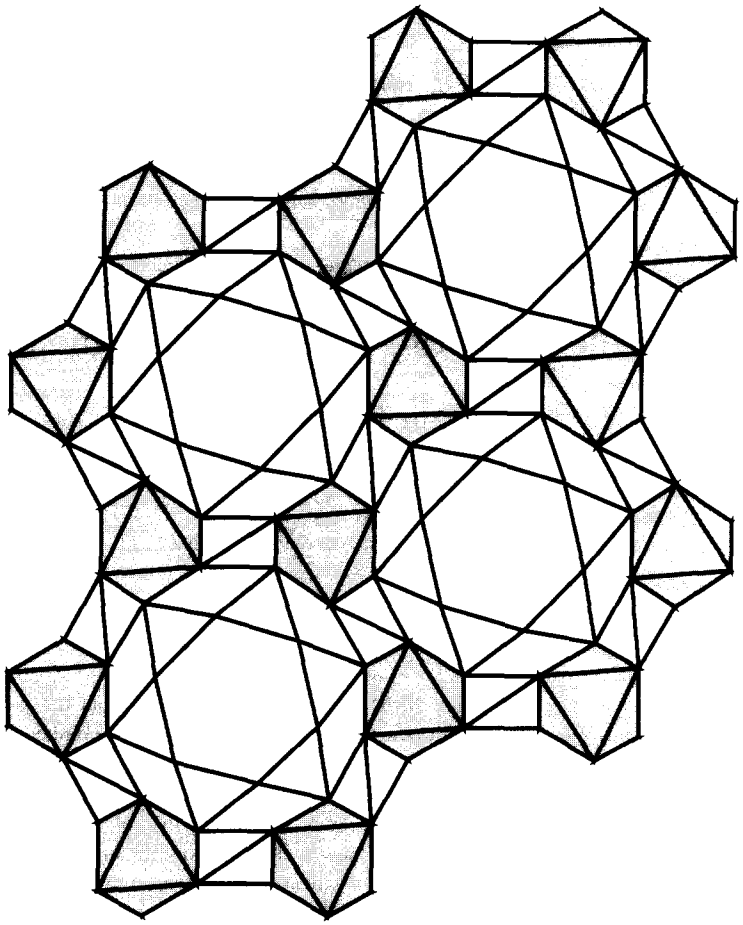

Fig. 1. The crystal structure of cordierite, $Mg_2Al_4Si_5O_{18}$, showing an infinite framework of linked SiO_4 and AlO_4 tetrahedra, together with an octahedral Mg site. The tetrahedra and octahedra are shown as shaded units. The view is down the [001] axis of the hexagonal structure. The structure is described in detail by Putnis (1992).

orientations of two linked tetrahedra, as described by the mean Si–O–Si (or Si–O–Al) bond angle. The second is the correlation with the number of AlO_4 tetrahedra linked to a single SiO_4 tetrahedron. These two correlations are illustrated in the MAS-NMR spectra for cordierite. Cordierite has two distinct tetrahedral sites, one in the six-membered rings seen in Fig. 1, and the second which provides a link between rings and which are located in four-membered rings; these are highlighted in Fig. 4. The existence of two distinct tetrahedral sites implies that there should be two groups of peaks in the MAS-NMR spectra following the correlation with the site topology. When cordierite is first prepared from a glass of the same composition, it has a disordered arrangement of the Al and Si cations within a hexagonal crystal structure, which is not entirely random

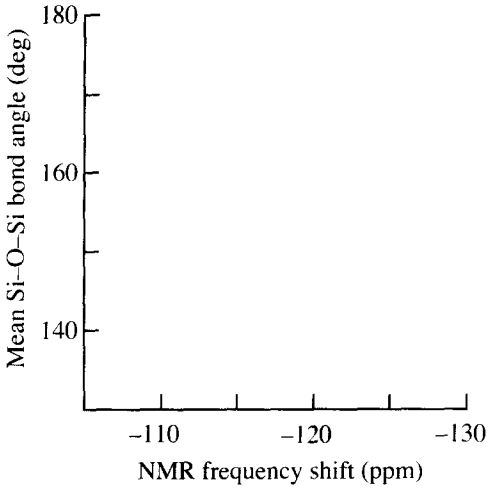

Fig. 2. Correlation of the ^{29}Si NMR frequency shift with the mean Si–O–Si bond angle. The broad band indicates the spread of experimental data (after Putnis, 1992).

since there is a preference for the Al cations to occupy the T1 sites (Putnis et al., 1985). On annealing, the cations order to produce an orthorhombic crystal structure, and the effects on the MAS-NMR spectra is shown in Fig. 5 (Putnis et al., 1985; Putnis and Angel, 1985). In the disordered phase the spectra for the different tetrahedral sites, T1 and T2, show a number of peaks corresponding to the different numbers of linked AlO_4 tetrahedra. On annealing the Al and Si cations order, so that in the most ordered state the spectra are dominated by just two peaks, the T1 SiO_4 tetrahedra linked to four AlO_4 tetrahedra, and the T2 SiO_4 tetrahedra linked to three AlO_4 tetrahedra and one SiO_4 tetrahedron.

Our own interest in the use of ^{29}Si MAS-NMR arises from the possibility to use the data to give information about the change in the order, and specifically

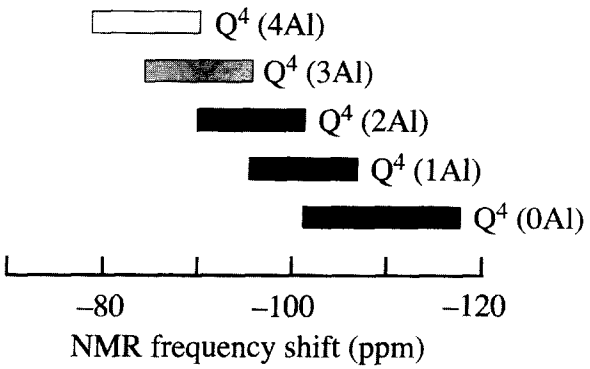

Fig. 3. Correlation of the ^{29}Si NMR frequency shift with the number of neighbouring AlO_4 tetrahedra. The broad bands indicate the spread of experimental data (after Putnis, 1992).

the change in the number of linked AlO_4 tetrahedra, on annealing through an ordering phase transition. A large part of modern mineralogy is concerned with understanding the behaviour of phase transitions in minerals, for it is now

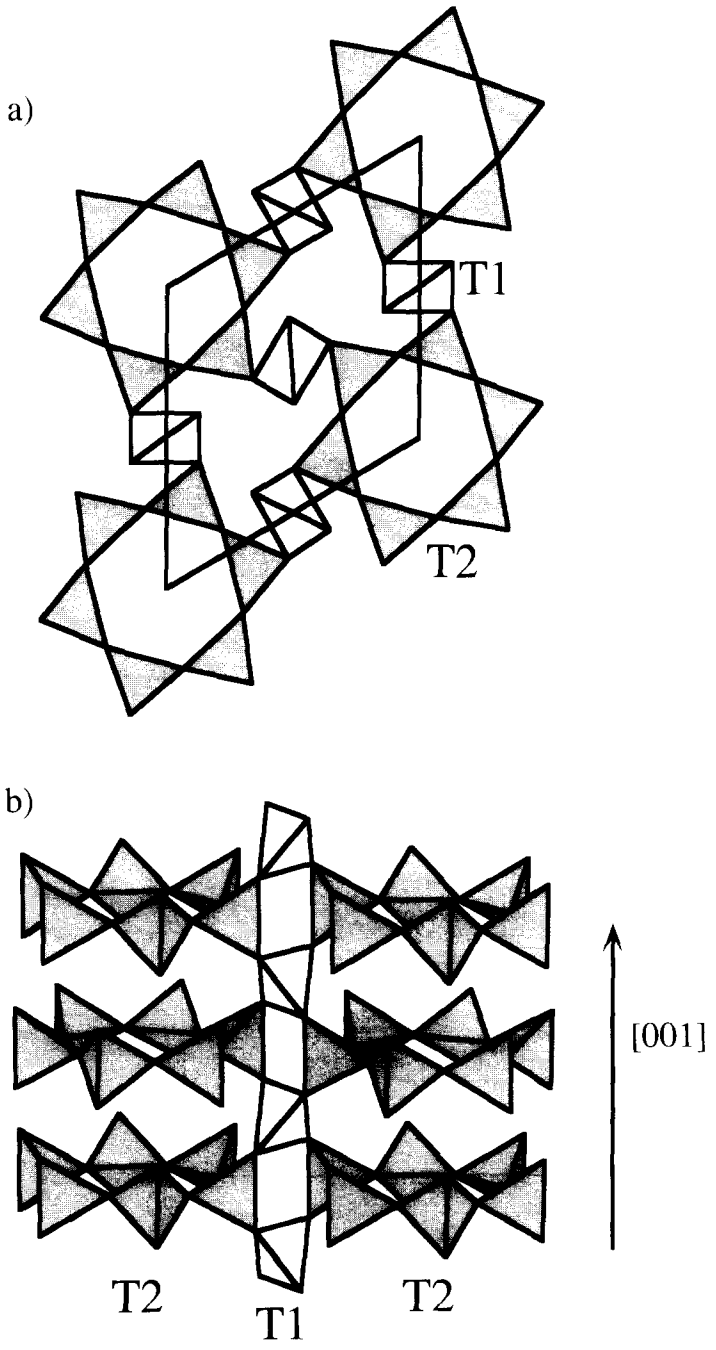

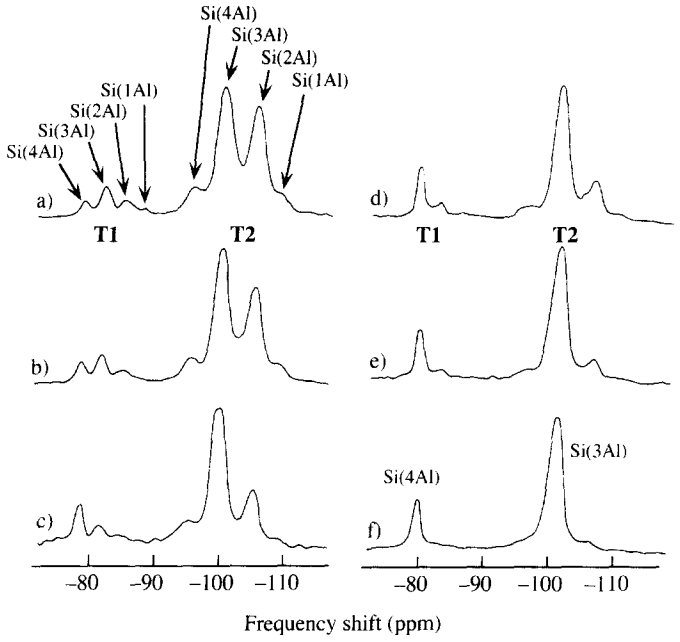

Fig. 5. ^{29}Si MAS-NMR spectra of cordierite during the annealing process, where the spectra (a–f) correspond to increasing annealing time, and hence increasing Al/Si order (Putnis et al., 1985; after Putnis, 1992). The assignments of the peaks are identified by the different tetrahedra and the different numbers of neighbouring AlO_4 tetrahedra.

recognised that there are important physical, chemical and thermodynamic consequences of the existence of these phase transitions. This point has been discussed in some detail by Putnis (1992). For Al/Si ordering, the change in enthalpy as a result of ordering can be of the order of 50 kJ mol^{-1}. As part of a larger project to understand these ordering transitions we have been calculating these ordering energies for a number of important examples (Bertram et al., 1990; Dove et al., 1993; Thayaparam et al., 1994, 1996). It is known that the ordering process is driven by the preference for Al cations to avoid occupying neighbouring tetrahedral sites (Loewenstein, 1954), and so we have been calculating the energies for the reactions Al–O–Al + Si–O–Si → 2(Si–O–Al). Our approach, in brief, has been to use large supercells of a given crystal structure, and to generate a large number (of around 100) of different configurations of the supercell with different distributions of the Al and Si cations

Fig. 4. Two views of the framework of linked tetrahedra in cordierite showing the T1 and T2 tetrahedra: (a) viewed down [001]; (b) viewed from a direction nearly normal to [001]. The tetrahedra are shown as shaded units, with T1 and T2 tetrahedra shown with different shadings. Note that the T2 tetrahedra lie in six-membered rings, and the T1 tetrahedra provide the bridging between neighbouring T2 rings. Each T1 tetrahedron is linked to four T2 neighbours, and each T2 tetrahedron is linked to two T1 and two T2 neighbours.

(Bertram et al., 1990; Thayaparam et al., 1994). For each configuration we calculate the lattice energy using a tested empirical potential (Winkler et al., 1991), allowing the atoms to move slightly to find the minimum of the energy. With a large number of configurations we can generate a data base of energy as a function of the number of Al...Al neighbours, taking account of second and third neighbours as well as nearest neighbours, from which we can extract the relevant interaction energies, as discussed by Bertram et al. (1990), Dove et al. (1993), and Thayaparam et al. (1994, 1996). A simple example is shown in Fig. 6, where we plot the energy against the number of nearest-neighbour Al...Al linkages for a number of different configurations of the Al and So tetrahedral cations in the mineral leucite, $KAlSi_2O_6$ (Dove et al., 1993). The best-fit straight line provides an estimate of the interaction energy, which in this case was 65 kJ mol^{-1}. For a number of examples we have found energies for nearest-neighbour interactions ranging from 40 to 120 kJ mol^{-1} (Dove et al., 1996). We have calibrated these energies against ab initio electronic structure calculations (Heine et al., 1997), and have performed extensive Monte Carlo simulations to study the evolution of ordering with temperature and time (Thayaparam et al., 1996; Dove et al., 1996). One of the issues that we have been investigating is to explain why the ordering temperatures for some silicates can be remarkably lower than would be predicted by a simple thermodynamic argument, but that is another story (Dove et al., 1996).

So, more specifically, our interest in the ^{29}Si MAS-NMR data arises from our need to link our theoretical studies with experiment. In principle the ^{29}Si MAS-NMR data contain information about the number of linked AlO_4 tetrahedra (Putnis and Angel, 1985). Our analysis of the theory makes predictions for this quantity (Thayaparam et al., 1996; Dove et al., 1996). In some cases we predict that this number is allowed to be very small in the disordered phase, and indeed it is this possibility to have complete Al...Al avoidance within the

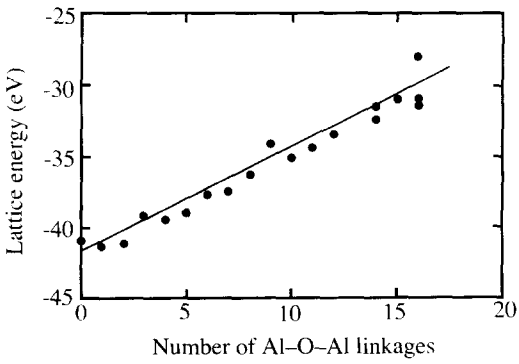

Fig. 6. Lattice energy plotted against the number of nearest-neighbour Al–O–Al linkages calculated for a number of different configurations of the Al and Si cations in the mineral leucite, $KAlSi_2O_6$, using the method described in the text (Dove et al., 1993).

disordered phase, leading to significant short-range order, that can give rise to extremely low ordering temperatures (Dove et al., 1996). In other cases, the evolution of the number of nearest-neighbour Al–O–Al linkages can be correlated with measurements of the enthalpy, so that it is possible to determine the energy required to form an Al–O–Al linkage experimentally. This has been done for cordierite (Carpenter et al., 1983; Putnis and Angel, 1985), and we had been hoping to use this work for cordierite to check our theoretical calculations (Thayaparam et al., 1996). Unfortunately, this is where we ran into the problems that form the central part of this contribution. For cordierite there are two types of nearest-neighbour pairs, T1–T2 and T2–T2, as seen in Fig. 5. The MAS-NMR data were initially analysed to sum the number of Al...Al neighbours over both types of neighbour pairs (Putnis and Angel, 1985). When we unpacked the equations to form separately the number of Al...Al linkages for both T1–T2 and T2–T2 neighbours, we found that for the more-ordered samples the number of Al...Al linkages for the T2–T2 neighbours came out with a negative value (Thayaparam et al., 1996). Whilst absurd, this simply reflects the fact that the numbers we want to extract involve subtracting two large numbers, so the final number is dominated by the errors, even when the data themselves appear to be of high quality. The point is that there is nothing in the simple analysis to constrain the number of neighbours to be positive. Following this, we developed a new method to analyse the ^{29}Si MAS-NMR data to incorporate the constraint that the number of neighbours must always be positive (Dove and Heine, 1996), and this is described in the next section. In the next section I will describe the application of the method to the analysis of ^{29}Si MAS-NMR data to the minerals leucite and analcime, as well as to cordierite.

2. Analysis method

The important experimental quantity in the ^{29}Si MAS-NMR spectra is the integrated intensity of each peak, which is proportional to the relative number of Si cations on the site of type j that have n Al neighbours, and which we denote by g_n^j. These are normalized to $\sum g_n^j$ (summing over both j and n). The objective is to determine a distribution of Al and Si cations that best fits the set of experimental values of g_n^j. We simulated a sample containing several unit cells of tetrahedral sites, set up with periodic boundaries in order to reduce finite size and surface effects, and then distribute the Al and Si cations over the tetrahedral sites using the experimental values of g_n^j as a guide. The quantity

$$\epsilon = \sum_n \sum_j \left[g_n^j(\text{obs}) - g_n^j(\text{calc}) \right]^2 / \sigma^2$$

defines how closely the distribution of cations in the simulation resembles the experimental distribution, where (obs) and (calc) denote the experimental and

calculated values respectively. σ is an average error on the experimental values of g_n^j. The best distribution of the Al and Si cations will be the one that minimises the value of ϵ. We allow the initial distribution to evolve towards the best distribution using a Monte Carlo approach. This is implemented by taking an initial distribution of Al and Si cations, which may be completely random or fully ordered. At the start a pair of Al and Si cations are selected at random. If switching their positions lowers the value of ϵ, this is carried out. Otherwise, their positions are switched according to a probability $\exp(-\beta\epsilon)$, where β is a parameter that is selected by the user. In the standard Monte Carlo method, ϵ would play the role of an energy, and β would play the role of the reciprocal of the temperature. The procedure of proposing and testing random switches of the positions of the Al and Si cations is repeated again and again, until ϵ oscillates in value about a minimum mean value. This method will produce the most random distribution of Al and Si cations that is consistent with the experimental data, with the constraint that the number of Al–O–Al linkages of all types must be positive. From the equilibrated configurations it is then an easy matter to calculate the number of Al–O–Al linkages. More details of the method and its implementation are given in Dove and Heine (1996).

It is worth commenting on the importance of the choice of starting configuration. In principle the Monte Carlo method will always find the optimum configuration consistent with the experimental data, but in practice it may take a long time to do so. If the optimum configuration is highly ordered, but the starting configuration is completely disordered, the simulation will immediately begin to order. However, it may get trapped for a long time in a state that is almost sufficiently ordered, but not quite. It is then possible that there are only a few permissible changes that can take the configuration towards the optimum configuration, and this will lead to the requirement for long simulation runs. In this case it is usually better to begin with an ordered configuration deduced from diffraction data, then allowing the simulation to disorder the configuration. For cases where there is partial order, experience showed that both ordered and disordered initial configurations could quickly be changed in the Monte Carlo procedure to similar optimum configurations with the correct degree of partial order.

3. Results

3.1. Cubic Cs-exchanged leucite and analcimes

The mineral leucite, $KAlSi_2O_6$, has a cubic structure above 960 K, and is tetragonal at lower temperatures (Palmer et al., 1997). In the cubic phase there is only one distinct tetrahedral site, so this phase must necessarily have a disordered arrangement of the Al and Si cations. The phase transition has nothing to

do with Al/Si ordering, and has a purely displacive mechanism (Dove et al., 1993). Our theoretical analysis suggests, though, that there will be significant short-range order in the disordered cubic phase, specifically such that neighbouring tetrahedral sites will not both be occupied by Al cations (Dove et al., 1993, 1996). High-temperature ^{29}Si MAS-NMR work has not been carried out on the cubic phase. Instead, most of the work has been carried out at room temperature (Brown et al., 1987; Murdoch et al., 1988; Phillips et al., 1989). This has proved to be extremely problematic. In the tetragonal phase there are three symmetrically distinct tetrahedral sites, but because they become equivalent in the cubic phase they are not very different. Each site will then give up to five peaks in the MAS-NMR spectra with weights determined by the proportions of Si sites with 4 Al neighbours down to 0 Al neighbours. Because the three sites are so similar,

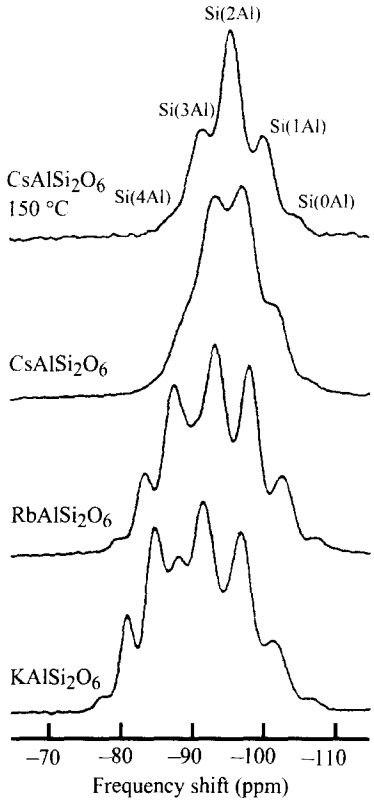

Fig. 7. ^{29}Si MAS-NMR spectra of leucite, $KAlSi_2O_6$, and the substituted materials $RbAlSi_2O_6$ and $CsAlSi_2O_6$ at room temperature, and $CsAlSi_2O_6$ in its cubic phase at 150°C. The spectrum for $CsAlSi_2O_6$ at 150°C contains five peaks associated with the sites with 0–4 Al neighbours, with only one symmetrically distinct tetrahedral site in the crystal structure. The other spectra contain up to fifteen overlapping peaks owing to the presence of three distinct, but similar, tetrahedral sites, with a disordered arrangement of Al and Si cations (after Phillips and Kirkpatrick, 1994).

all the NMR peaks overlap, and it has not been possible to interpret the spectra consistently. This problem is illustrated in Fig. 7. If the K cations are replaced by Cs, the transition temperature is lowered to 100°C (Palmer et al., 1997), and ^{29}Si MAS-NMR spectra from this phase are easier to obtain (Phillips and Kirkpatrick, 1994). Now there are only five peaks associated with a single tetrahedral site, as seen in Fig. 7. Moreover, there is a related mineral analcime, $NaAlSi_2O_6.H_2O$, where the water molecules replace the site occupied by the K cations in leucite, and the Na cations occupy smaller sites with a 2/3 probability. This structure is cubic, or close to cubic, at all temperatures (e.g. Line et al., 1996), and is shown in Fig. 8. Phillips and Kirkpatrick (1994) have measured the ^{29}Si MAS-NMR spectra for a suite of samples of analcime with varying Si:Al ratios. These are shown in Fig. 9: what is striking is that although the peaks are in more-or-less the same positions, the relative heights vary substantial between different samples.

The results of our inverse Monte Carlo simulations of the Al/Si distributions in the Cs-exchanged leucite and the different analcime samples are given in Table 1. The simulations had a cubic supercell of $2 \times 2 \times 2$ unit cells, containing 384 tetrahedral sites. The simulation of Cs-exchanged leucite shows that there is short-range order leading to a complete absence of Al–O–Al linkages, as we had predicted. On the other hand, the simulations of the different analcime samples showed the existence of some Al–O–Al linkages, but the number is

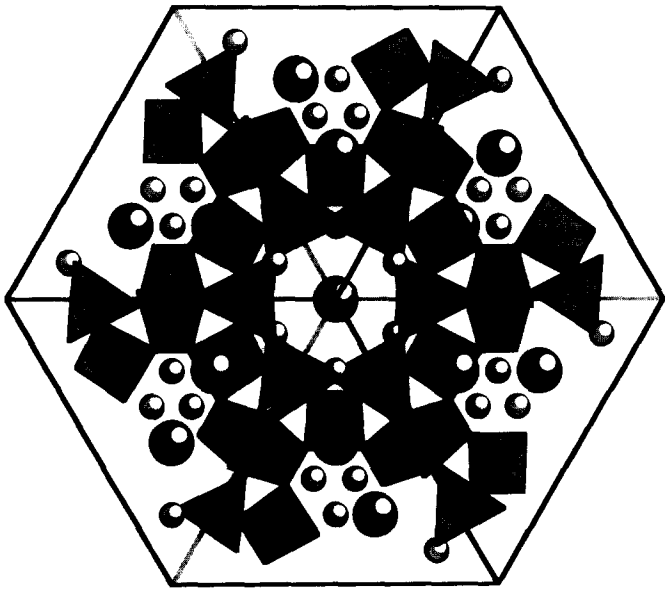

Fig. 8. Crystal structure of analcime, $NaAlSi_2O_6.H_2O$, viewed down [111], showing the framework of linked tetrahedra, the central positions occupied by the water molecules, and the sites occupied by the Na cations. The positions of the hydrogen atoms are disordered and no attempt has been made to indicate their distribution in this figure.

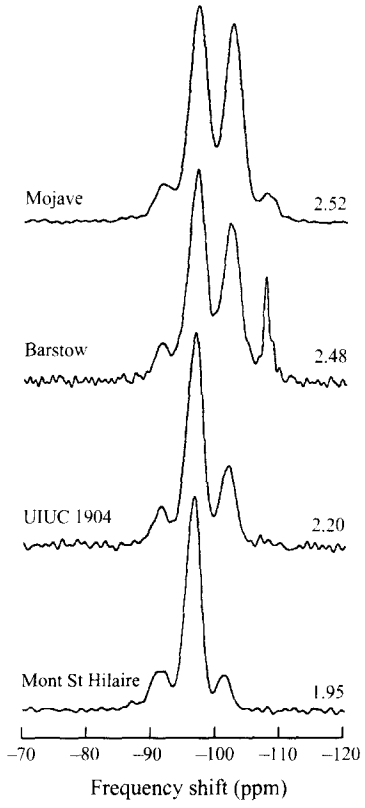

Fig. 9. ^{29}Si MAS-NMR spectra of different samples of the mineral analcime, $NaAlSi_2O_6.H_2O$. The samples have slightly different Si:Al ratios (given to the right of each spectrum), and different thermal histories (after Phillips and Kirkpatrick, 1994).

small compared to the number there would be if there was a completely random distribution of the Al and Si cations, $\sim 2/3$ per formula unit, implying that there is still a considerable degree of short-range order. The NMR spectra of the different analcime samples have significant differences, which are accounted for fully in the simulations.

3.2. Cordierite

The ^{29}Si MAS-NMR for cordierite are shown for different annealing times (Putnis, 1992) in Fig. 5. The integrated signals from the two sets of peaks indicated that the six T1 sites contain more Al than Si and that the twelve T2 sites contain less Al than Si at each stage in the annealing process. The ^{29}Si MAS-NMR data show that the sample progressively orders on annealing. The structure transforms from the initial hexagonal phase to a state with a characteristic tweed microstructure, and eventually an orthorhombic structure is formed with long-range Al/Si order (Putnis, 1992). The ^{29}Si MAS-NMR data change

Table 1
Experimental and calculated ^{29}Si MAS-NMR spectra (given as the relative integrated intensities of the peaks in the NMR spectra) for cubic Cs-exchanged leucite and various analcime samples (the last column gives the number of Al–O–Al linkages per formula unit)

	N_{Si}	g_0	g_1	g_2	g_3	g_4	$N_{Al-O-Al}$
Cs-leucite [a]							
Experimental	2.0	0.038	0.221	0.427	0.277	0.037	
Calculated		0.047	0.227	0.430	0.273	0.023	0
Analcime (Mont Saint Hilaire) [a]							
Experimental	1.95	0.010	0.122	0.695	0.157	0.016	
Calculated		0.024	0.122	0.693	0.154	0.008	0.09
Analcime (UIUC 1904) [a]							
Experimental	2.18	0.023	0.239	0.619	0.119	0.0	
Calculated		0.027	0.243	0.616	0.114	0.0	0.05
Analcime (Barstow) [a]							
Experimental	2.53	0.077	0.365	0.463	0.090	0.005	
Calculated		0.076	0.367	0.462	0.091	0.004	0.02
Analcime (Mojave) [a]							
Experimental	2.52	0.058	0.402	0.446	0.087	0.008	
Calculated		0.062	0.404	0.447	0.084	0.004	0.05
Analcime (Murdoch) [b]							
Experimental	2.13	0.020	0.234	0.597	0.148	0.0	
Calculated		0.023	0.234	0.594	0.149	0.0	0.03

[a] Experimental data are from Phillips and Kirkpatrick (1994). Average errors are ± 0.005.
[b] Experimental data are from Murdoch et al. (1988). Average errors are ± 0.003.

continuously through these transformation processes (Putnis et al., 1987), showing no signs of the formation of the tweed microstructure that is seen in the electron microscope as an intermediate stage in the ordering process, or the eventual transition to the orthorhombic phase.

The inverse Monte Carlo simulations were performed using a supercell made from a block of $2 \times 2 \times 2$ orthorhombic unit cells containing 288 tetrahedra. We also used both ordered and disordered starting points. For the most ordered samples the use of a disordered starting point led to the need for extremely long simulation runs, but the simulations with less order led to similar results for both types of starting configuration. The results of our simulations for different annealing times are given in Table 2, and the results of the analysis of the simulation configurations are given in Table 3. The changes in the ordering on annealing are very clear. One important point from the results is that there are virtually no Al–O–Al linkages of the form T2–T2. This result had been anticipated from our previous analysis of the ^{29}Si MAS-NMR data, where in each case we obtained a negative number for this quantity (Thayaparam et al.,

Table 2
Experimental and calculated ^{29}Si MAS-NMR spectra (given as the relative integrated intensities of the peaks in the NMR spectra) for cordierite with different annealing times; experimental data are from Putnis et al. (1985)

	g_0^1	g_1^1	g_2^1	g_3^1	g_4^1	g_0^2	g_1^2	g_2^2	g_3^2	g_4^2
2 min										
exp	0.0	0.006	0.042	0.053	0.020	0.0	0.049	0.347	0.408	0.075
calc	0.0	0.006	0.044	0.050	0.025	0.0	0.050	0.350	0.406	0.069
6.5 min										
exp	0.0	0.0	0.032	0.053	0.033	0.0	0.065	0.343	0.397	0.077
calc	0.0	0.0	0.031	0.056	0.031	0.0	0.063	0.344	0.394	0.081
23 min										
exp	0.0	0.0	0.038	0.058	0.037	0.0	0.052	0.308	0.428	0.079
calc	0.0	0.0	0.038	0.056	0.038	0.0	0.056	0.306	0.4250	0.081
6 h										
exp	0.0	0.011	0.022	0.043	0.080	0.0	0.020	0.203	0.513	0.108
calc	0.0	0.006	0.019	0.050	0.094	0.013	0.025	0.200	0.506	0.088
23.5 h										
exp	0.0	0.013	0.012	0.039	0.098	0.0	0.022	0.177	0.568	0.069
calc	0.0	0.006	0.013	0.044	0.100	0.013	0.025	0.175	0.563	0.063
48.5 h										
exp	0.0	0.003	0.010	0.023	0.114	0.0	0.020	0.143	0.625	0.061
calc	0.0	0.0	0.013	0.025	0.125	0.006	0.025	0.144	0.613	0.050
96 h										
exp	0.0	0.008	0.015	0.029	0.117	0.0	0.013	0.111	0.645	0.062
calc	0.0	0.006	0.013	0.038	0.125	0.013	0.019	0.106	0.638	0.044
408 h										
exp	0.0	0.008	0.016	0.018	0.131	0.0	0.014	0.056	0.672	0.084
calc	0.0	0.0	0.019	0.025	0.150	0.013	0.025	0.050	0.663	0.056
2000 h										
exp	0.0	0.0	0.014	0.027	0.144	0.0	0.0	0.059	0.698	0.058
calc	0.0	0.006	0.013	0.031	0.150	0.013	0.006	0.056	0.694	0.031

1996). In Table 3 we compare the calculated number of Al–O–Al linkages with the number computed directly from the experimental data by Putnis and Angel (1985). The agreement is reasonably good for short annealing times, but for longer annealing times the number given by Putnis and Angel (1985) is consistently lower than the value obtained in our simulations. This is because the numbers of Al–O–Al linkages obtained directly from the experimental data contain a significant negative number of T2–T2 linkages, which is larger for the longer annealing times. The simulations are constrained to avoid this negative

Table 3
Analysis of the simulated ensembles of cordierite

Annealing time	Fractional occupancy by Al		Number of Al–O–Al linkages		
	T1	T2	T1–T2	T2–T2	Putnis
2 min	0.79	0.27	1.53	0	1.51
6.5 min	0.80	0.27	1.41	0.13	1.49
20 min	0.78	0.28	1.34	0	1.33
6 h	0.72	0.31	0.84	0	0.74
23.5 h	0.73	0.30	0.81	0	0.74
48.5 h	0.73	0.30	0.63	0	0.56
96 h	0.70	0.32	0.59	0	0.47
408 h	0.68	0.33	0.38	0	0.26
2000 h	0.67	0.33	0.38	0	0.18

The data in the last column are from Putnis and Angel (1985), and include both the T1–T2 and T2–T2 linkages. The number of Al–O–Al linkages are given per tetrahedron.

contribution to the number of Al–O–Al linkages. Fig. 10 gives the number of Al–O–Al linkages calculated in our simulations as a function of the logarithm of the annealing time. The plot is linear within the experimental errors, with a gradient of $\partial N/\partial \log_{10}(t) \approx -0.25$. Comparing these results with the calorimetric data of Carpenter et al. (1983) leads to a value for the energy of the reaction (Al–O–Al) + (Si–O–Si) ⇒ 2 (Al–O–Si) of ~ 40 kJ/mol. This value is lower than the value we obtained from our theoretical calculations (Thayaparam et al., 1996). One problem is that we have not taken account of the preference of the Al for the T1 sites at short annealing times, with an excess of Al in T1 over the expected occupancy of 2/3. Since the partitioning of the Al cations over the T1 and T2 sites changes with annealing time, the changes in enthalpy will include this contribution, but it is not likely that this accounts for all of the discrepancy. Alternatively, there is a clue from Table 2. The

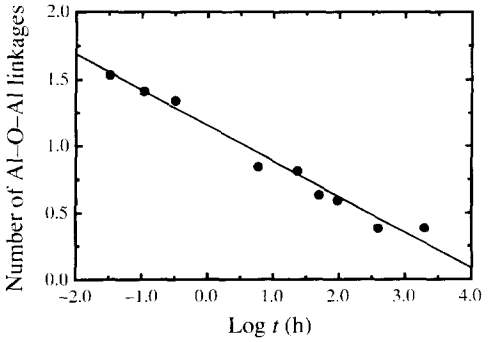

Fig. 10. Plot of number of Al–O–Al linkages in cordierite as a function of the logarithm of annealing time, as obtained from our inverse Monte Carlo simulations. The straight line is fitted to the data.

experimental data give $g_0^2 = 0$ for all spectra (this is the T2 peak for the Si cation having no Al neighbours), whereas the simulations suggest that $g_0^2 \neq 0$. We have explored the effects of including a non-zero value for both g_0^2 and g_0^1, and we have found that the final number of Al–O–Al linkages is very sensitive to the existence of non-zero values of these quantities (Dove and Heine, 1996). Indeed, with only a very small intensity for these peaks the change in slope of the plot in Fig. 10 can lead to a new value for the ordering energy that is in good agreement with our theoretical calculations. More recent data (A. Putnis, pers. commun.) have shown the existence of a small Si(0Al) T2 peak as our inverse Monte Carlo simulations have predicted.

4. Discussion

The examples discussed in this paper show the power and sensitivity of the ^{29}Si MAS-NMR method to provide detailed information about short-range structural order in silicates with long-range Al/Si disorder. The peak frequencies are correlated both to the structural topology and the number of neighbouring AlO_4 tetrahedra. In cases such as the tetragonal phase of leucite, where as a result of the displacive phase transition the different tetrahedral sites are similar, it may not be possible to accurately assign all the overlapping peaks. On the other hand, even with a spectrum containing peaks that are properly resolved, there may be other problems. For example, in the determination of the number of Al–O–Al linkages, the result by simply applying equations may be dominated by the errors on the data, even for high-quality data. The equations do not constrain these numbers to be positive, even though the possibility of negative numbers is physically absurd. As a result we developed the inverse Monte Carlo method described in this article. Our analysis highlighted another problem, namely that it is essential that all peaks are identified, even if their intensities are very low. Small errors associated with missing peaks can skew the final analysis to an unacceptable degree.

Acknowledgements

I am extremely grateful for the collaboration with Volker Heine, S. Thayaparam, Kenton Hammonds and Eva Myers in our theoretical analysis of the problem of Al/Si ordering in minerals, and also for discussions with Andrew Putnis about the NMR data on cordierite. I would like to thank the organisers of the symposium for the invitation to contribute. Finally, I would like to thank my wife, Kate, and my three daughters: this was my last journey of a summer that was more busy than usual, and they were supportive to the last.

References

Bertram, U.C., Heine, V., Leslie, M., Price, G.D., 1990. Computer modelling of Al/Si ordering in sillimanite. Phys. Chem. Miner. 17, 326–333.

Brown, I.W.M., Cardile, C.M., MacKenzie, K.J.D., Ryan, M.J., Meinhold, R.H., 1987. Natural and synthetic leucites studied by solid state 29-Si and 27-Al NMR and 57-Fe Mossbauer spectroscopy. Phys. Chem. Miner. 15, 78–83.

Carpenter, M.A., Putnis, A., Navrotsky, A., McConnell, J.D.C., 1983. Enthalpy effects associated with Al,Si ordering in anhydrous Mg-cordierite. Geochim. Cosmochim. Acta 47, 899–906.

Dove, M.T., Heine, V., 1996. The use of Monte Carlo methods to determine the distribution of Al and Si cations in framework aluminosilicates from ^{29}Si MAS-NMR data. Am. Mineral. 81, 39–44.

Dove, M.T., Cool, T., Palmer, D.C., Putnis, A., Salje, E.K.H., Winkler, B., 1993. On the role of Al–Si ordering in the cubic-tetragonal phase transition in leucite. Am. Mineral. 78, 486–492.

Dove, M.T., Thayaparam, S., Heine, V., Hammonds, K.D., 1996. The phenomenon of low Al–Si ordering temperatures in aluminosilicate framework structures. Am. Mineral. 81, 349–362.

Heine, V., Dove, M.T., De Vita, A., Ortega, J., Myers, E., 1997. Computational studies of Si/Al ordering in aluminosilicate framework structures. Phase Transitions (in press).

Kirkpatrick, R.J., 1988. MAS NMR spectroscopy of minerals and glasses. Rev. Mineral. 18, 341–403.

Line, C.M.B., Dove, M.T., Knight, K.S., Winkler, B., 1996. The low-temperature behaviour of analcime, I. High-resolution neutron powder diffraction. Mineral. Mag. 60, 499–507.

Loewenstein, W., 1954. The distribution of aluminium in the tetrahedra of silicates and aluminates. Am. Mineral. 39, 92–96.

Murdoch, J.B., Stebbins, J.F., Carmichael, I.S.E., Pines, A., 1988. A silicon-29 nuclear magnetic resonance study of silicon–aluminium ordering in leucite and analcite. Phys. Chem. Miner. 15, 370–382.

Palmer, D.C., Dove, M.T., Ibberson, R.M., Powell, B.M., 1997. Structural behavior, crystal chemistry and phase transitions in substituted leucites: high-resolution neutron powder diffraction. Am. Mineral. 82, 16–30.

Phillips, B.L., Kirkpatrick, R.J., 1994. Short-range Si–Al order in leucite: determination of the configurational entropy from ^{27}Al and variable-temperature ^{29}Si NMR spectroscopy of leucite, its Cs- and Rb-exchanged derivatives and analcime. Am. Mineral. 79, 1025–1031.

Phillips, B.L., Kirkpatrick, R.J., Putnis, A., 1989. Si,Al ordering in leucite by high-resolution ^{27}Al MAS NMR spectroscopy. Phys. Chem. Miner. 16, 591–598.

Putnis, A., 1992. Introduction to Mineral Sciences. Cambridge University Press, Cambridge.

Putnis, A., Angel, R.A., 1985. Al,Si ordering in cordierite using 'magic angle spinning' NMR, II. Models of Al,Si order from NMR data. Phys. Chem. Miner. 12, 217–222.

Putnis, A., Fyfe, C.A., Gobbi, G.C., 1985. "Al,Si ordering in cordierite using 'magic angle spinning' NMR, I. Si^{29} spectra of synthetic cordierites. Phys. Chem. Miner. 12, 211–216.

Putnis, A., Salje, E., Redfern, S., Fyfe, C.A., Strobl, H., 1987. Structural states of Mg-cordierite, I. Order parameters from synchrotron X-ray and NMR data. Phys. Chem. Miner. 14, 446–454.

Thayaparam, S., Dove, M.T., Heine, V., 1994. A computer simulation study of Al/Si ordering in gehlenite and the paradox of low transition temperature. Phys. Chem. Miner. 21, 110–116.

Thayaparam, S., Heine, V., Dove, M.T., Hammonds, K., 1996. A computational study of Al/Si ordering in cordierite. Phys. Chem. Miner. 23, 127–139.

Winkler, B., Dove, M.T., Leslie, M., 1991. Static lattice energy minimisation and lattice dynamics calculations on aluminosilicate minerals. Am. Mineral. 76, 313–331.